Coordinated Power Control of PV Generation, Electric Mobility and Electric Heating in Different Grids

Damianakis, Nikolaos; Mouli, Gautham Ram Chandra; Yu, Yunhe; Bauer, Pavol

DOI
10.1109/IPEMC-ECCEAsia60879.2024.10567854

Publication date
2024

Document Version
Final published version

Published in
2024 IEEE 10th International Power Electronics and Motion Control Conference, IPEMC 2024 ECCE Asia

2024 IEEE 10th International Power Electronics and Motion Control Conference (IPEMC2024-ECCE Asia) | 979-8-3503-5133-0/24/$31.00 ©2024 IEEE | DOI: 10.1109/IPEMC-ECCEAsia60879.2024.10567854

Coordinated Power Control of PV Generation, Electric Mobility and Electric Heating in Different Grids

1st Nikolaos Damianakis
Electrical Sustainable Energy
Delft University of Technology
Delft, Netherlands
N.Damianakis@tudelft.nl

2nd Gautham Ram Chandra Mouli
3rd Yunhe Yu
Electrical Sustainable Energy
Delft University of Technology
Delft, Netherlands
G.R.ChandraMouli@tudelft.nl

4th Pavol Bauer
Electrical Sustainable Energy
Delft University of Technology
Delft, Netherlands
P.Bauer@tudelft.nl

***Abstract*—Power control of flexible loads will play a significant role in energy transition. This work has developed a mixed-integer linear power control (MILP) model that manages electric vehicle (EV) chargers, heat pumps (HPs), and PV rooftops. The power control was tested with and without vehicle-to-grid (V2G) capabilities in different grid types, namely residential, commercial, and mixed grids. Moreover, the effect of different seasons and charger efficiencies was investigated. It was shown that grid characteristics such as EV parking times and building occupations can affect significantly the power control, e.g. the amount of imported and V2G power. Moreover, while V2G power is rarely used due to current V2G round-trip efficiency, future efficiency improvement can lead to a significant increase in V2G use. Finally, the seasonal effect had also a significant impact with Summer being characterized by higher exported and lower imported energy due to the high and prolonged PV power availability.**

***Index Terms*—power control, PV, electric vehicles, heat pumps, energy hubs, V2G**

I. Introduction

Energy transition will cause an abrupt increase in distributed generation such as PVs and electric load demand such as electric heating and mobility. However, several negative impacts on the distribution grid are foreseen if their operation is performed uncontrollably, e.g. power peaks, voltage violations, component overloading, etc [1]. Therefore, the power control of PV generation, heat pumps (HPs), and electric vehicles (EVs) will play a significant role in the energy transition of future distribution grids [2]. Furthermore, the vehicle-to-grid (V2G) capabilities of the EVs are currently drawing high attention due to the fast response of the EVs for both the power scheduling of future energy management systems (EMSs) and provision of ancillary services such as congestion management, peak shaving, etc [3], [4]. However, the V2G use has the drawback of power losses due to the charger's round-trip efficiency. Finally, EMSs will appear in different sectors of future distribution grids with different characteristics [1]. For example, the residential sector comprises mostly "Home" chargers while the commercial sector comprises "Semi-Public" and "Public" chargers which are characterized by different requested amounts of energy and parking times. Moreover, the occupancy periods of the residential and commercial buildings highly differ both during weekdays and weekends.

with project number 17628 of the research program Crossover, which is (partly) financed by the Dutch Research Council (NWO)

II. Literature Review & Contributions

The authors in [5], [6] developed two-stage EMSs to cope with the uncertainties of day-ahead (DA) and real-time (RT) power scheduling such as PV generation and load demand. Moreover, a three-stage mixed-integer linear programming (MILP) model was developed in [7] which also participated in the wholesale market considering the EV battery degradation. However, all three studies did not consider the effect of HPs on power scheduling. The trade-off between minimum power control cost of PVs, EVs, and HPs compared to battery degradation was investigated in the probabilistic study of [8] while a related comparison of four different power control techniques was performed in [2]. However, the V2G effect was not investigated in both of these studies. The studies in [9] and [10] incorporated the V2G effect in their power scheduling, showing that V2G can still be cost-effective if it is managed optimally, however, they both remained on a building level. Concerning grid-level studies, the V2G effect on peak-shaving and congestion management has been studied in [3] & [4], respectively, however, the impact of the grid case characteristics was not evaluated. Finally, 5 different LV networks were analyzed in [1] to enhance the HP hosting capacity with the use of EV smart-charging and V2G.

However, the impact of charger efficiencies and different grid characteristics such as EV parking times and buildings' occupancy on power control and V2G use has not yet been investigated. In this work, a power control model is developed that controls EV charging, PV rooftop generation & HP heating/cooling. The major contributions are the comparison of power scheduling with and without V2G at different grids (residential, commercial, and mixed), hereby named "nodes"

979-8-3503-5133-0/24/$31.00 ©2024 IEEE

due to their small size compared to the main grid, and seasons. Moreover, V2G use is tested evaluating its current and future potential in power scheduling depending on current and future V2G efficiencies. Hence, the contributions can be summarized as follows:

1) Development of a power control model that manages PV generation, electric mobility, and electric heating with and without V2G capabilities.

2) Comparison of the model performance regarding V2G use and grid power exchange under different grid characteristics, EV charger efficiencies, and seasons.

III. Coordinated Power Control Methodology

This section comprises the model of the MILP coordinated power control which is divided into EV charging, building, and node constraints.

A. EV Charging Constraints

The EV charging constraints of the power control model listed below are based on [11], and the indices n, j, t, T, a, d represent the node, charger, time instant, optimization horizon, arrival, and departure, respectively. It must be noted that V2G currently is intended to be used only for DC chargers due to the elimination of the AC-DC converters in the G2V and V2G power flow and the increased efficiency [10]. In this work, the reasoning behind using V2G in AC charging is twofold. Firstly, we intend to use the same example for power control with and without V2G to realize a fair comparison. Secondly, we assume that the power conversion losses can further decrease in the future and V2G be more efficiently integrated into EV AC charging.

$$P_{ch}^{n,j,t} = \Phi^{n,j} I_{ch}^{n,j,t} V^{n,t} \quad \forall t \in T \tag{1}$$

$$P_{v2g}^{n,j,t} = \Phi^{n,j} I_{v2g}^{n,j,t} V^{n,t} \quad \forall t \in T \tag{2}$$

$$0 \leq P_{ch}^{n,j,t} \leq P_{ch_{max}}^{n,j} \;\&\; 0 \leq I_{ch}^{n,j,t} \leq I_{ch_{max}}^{n,j} \quad \forall t \in T \tag{3}$$

$$0 \leq P_{v2g}^{n,j,t} \leq P_{v2g_{max}}^{n,j} \;\&\; 0 \leq I_{v2g}^{n,j,t} \leq I_{v2g_{max}}^{n,j} \quad \forall t \in T \tag{4}$$

Equation (1) dictates the EV charging power where $I_{ch}^{n,j,t}$ the instantaneous phase charging current, $\Phi^{n,j}$ the number of phases for charging the particular EV, and $V^{n,t}$ the node voltage assumed steady at 230V. Similarly, (2) describes the EV V2G power where $I_{v2g}^{n,j,t}$ the instantaneous phase V2G current. The limits of charging and V2G power and current are dictated in (3) & (4) which depend on the rated EV and EV charger specifications (see also TABLE I).

$$B^{n,j,t} = B_a^{n,j} + \Delta t \sum_{T_a^{n,j}}^{t} (P_{ch}^{n,j,t} h_{ev}^{n,j} - \frac{P_{v2g}^{n,j,t}}{h_{ev}^{n,j}}) \;\; \forall t \in [T_a^{n,j}, T_d^{n,j}] \tag{5}$$

$$S^{n,j,t} = \frac{B^{n,j,t}}{B_{max}^{n,j} - B_{min}^{n,j}} \quad \forall t \in T \tag{6}$$

$$B^{n,j,t}, I_{ch}^{n,j,t}, I_{v2g}^{n,j,t} = 0 \quad \forall t \notin [T_a^{n,j}, T_d^{n,j}] \tag{7}$$

The EV battery capacity dynamics $B^{n,j,t}$ are modeled in (5) where $T_a^{n,j}$, $T_d^{n,j}$ & $B_a^{n,j}$ the EV arrival time, departure time & arrival capacity, and $h_{ev}^{n,j}$ the EV battery management system (BMS) efficiency. Since the power is measured before the EV BMS, $h_{ev}^{n,j}$ is used inversed for the calculation of the V2G power. The EV SOC dynamics are modeled in (6) which depend on the maximum and minimum battery capacity $B^{n,j}$. Moreover, no V2G and charging are realized outside the EV parking time in (7).

$$b_{ch}^{n,j,t} + b_{v2g}^{n,j,t} \leq 1 \quad \forall t \in T \tag{8}$$

$$P_{ch}^{n,j,t} \leq b_{ch}^{n,j,t} P_{ch_{max}}^{n,j} \quad \forall t \in T \tag{9}$$

$$P_{v2g}^{n,j,t} \leq b_{v2g}^{n,j,t} P_{v2g_{max}}^{n,j} \quad \forall t \in T \tag{10}$$

Equations (8) - (10) dictate that charging power P_{ch} and V2G power P_{v2g} cannot be realized simultaneously. Firstly binary variables $b_{ch}^{n,j,t}$ & $b_{v2g}^{n,j,t}$ are introduced for charging and V2G power, respectively, which activate only one mode at a time. In (9) - (10), they are connected with $P_{ch}^{n,j,t}, P_{v2g}^{n,j,t}$ respectively, to be incorporated in a MILP EMS.

$$E_g^{n,j} = B_a^{n,j} + d^{n,j} - B_d^{n,j} \tag{11}$$

Finally, (11) dictates the unfinished charging gap which is calculated by subtraction of the departure capacity $B_d^{n,j}$ from the sum of the arrival capacity $B_a^{n,j}$ and the requested energy $d^{n,j}$. This gap induces penalty cost for the EMS to be paid to the EV owners and, thus, it is incorporated in the cost minimization of the objective function (see IIIC. node constraints).

B. Building Constraints

The constraints of the power control model concerning the PV generation and HP heating/cooling of the buildings listed below are based on [12] where b, surf denote the building and surface, respectively. All the following constraints apply for $\forall t \in T$.

$$T^{n,b,t} = T_{st}^{n,b} + \Delta t \sum_{t_{st}}^{t} \frac{Q_{tot}^{n,b,t}}{C_b + V_b C_{air} \rho_{air}} \tag{12}$$

$$Q_{tot}^{n,b,t} = Q_{hp}^{n,b,t} m^{n,b} + I_r^{n,b,t} - Q_{los}^{n,b,t} \tag{13}$$

$$Q_{los}^{n,b,t} = (\sum_{sf} U_{sf} A_{sf} + C_{air} \;\rho_{air}\; r_b)(T^{n,b,t} - T_a^t) \tag{14}$$

The building temperature dynamics $T^{n,b,t}$ are modeled in (12) which depend on the total heating gains and losses Q_{tot} divided by the total building thermal capacity, This is the sum of the thermal capacity of the building mass C_b and the capacity of the building air where V_b, C_{air}, and ρ_{air} the building volume, the air specific capacity and air density, respectively. Equation (13) denotes that Q_{tot} comprise the HP

heating output Q_{hp}, the heating gains from irradiation I_r and the total heating losses Q_{los} where m denotes the HP mode (+1 for heating & -1 for cooling). The total heating losses Q_{los} depend on the conduction losses (first term) and ventilation losses (second term) as shown in (14). The former depends on the sum of the conductivity U over the area A of every building surface while the latter depends on the building air change rate r. Both of them depend also on the difference between the instantaneous building temperature and ambient Temperature T_a.

$$P_{hp}^{n,b,t} = \frac{Q_{hp}^{n,b,t}}{c_{p_{hp}}^{n,b,t}} \tag{15}$$

$$\begin{aligned} T_{min}^{n,b} \leq T^{n,b,t} \leq T_{max}^{n,b} \\ 0 \leq Q_{hp}^{n,b,t} \leq Q_{hp_{max}}^{n,b} \\ 0 \leq P_{hp}^{n,b,t} \leq P_{hp_{max}}^{n,b} \end{aligned} \tag{16}$$

Moreover, (15) dictates the HP power consumption where $c_{p_{hp}}$ represents the HP Coefficient of Performance (COP) which for the needs of this work has been assumed steady. The limits of the building temperature, HP heating output, and HP power consumption are modeled in (16). In [12], the calculation of the heating gains by building incident irradiation is described which depends also on the window-to-wall ratio (WWR) of the buildings and the solar-heat-gain-coefficient (SHGC) of the building windows (both assumed 0.2).

$$P_{pv_{dev}}^{n,b,t} = P_{pv_{max}}^{n,b,t} - P_{pv_{use}}^{n,b,t} \text{ where } 0 \leq P_{pv_{use}}^{n,b,t} \leq P_{pv_{max}}^{n,b,t} \tag{17}$$

$$\begin{aligned} T_{dev}^{n,b,t} = \max(T^{n,b,t} - T_{high}^{n,b}, T_{low}^{n,b} - T^{n,b,t}, 0) \Leftrightarrow \\ T_{dev}^{n,b,t} = \max(\max(T^{n,b,t} - T_{high}^{n,b}, T_{low}^{n,b} - T^{n,b,t}), 0) \end{aligned} \tag{18}$$

In this work, the EMS is assumed to control the PV rooftop generation and the HP heating/cooling of every building at every time instant. Hence, the EMS is modeled to avoid PV curtailment of the PV owners as well as to respect the buildings' thermal comfort. Therefore, along with the penalty cost for the unfinished EV charging that was explained before, the objective function also integrates penalty costs for PV curtailment and thermal comfort violation. These costs are dependent on the difference between the used PV power and the PV generation and between the building temperature and the desired temperature levels every time instant.

The instantaneous PV curtailment amount is dictated in (17) where $P_{pv_{max}}$ & $P_{pv_{use}}$ the PV generation and used PV power, respectively. The temperature deviation T_{dev} is defined in (18) as the temperature difference from the nearest desired temperature interval limit $T_{low}^{n,b}$ or $T_{high}^{n,b}$ (see TABLE I). However, (18) is not a linear constraint and cannot be integrated as is in the power control which is a MILP model. It is well known that a min or max equation can be linearized by applying the big-M method. Dividing (18) into two max functions and applying the big-M method twice, 3 new support decision variable series $y_{T_{dev}}, z_{T_{dev}}, c_{T_{dev}}$ and 2 M constants M1 & M2 are introduced and the linearization of (18) is realized by (19) - (25).

$$y_{T_{dev}}^{n,b,t} \geq T^{n,b,t} - T_{high}^{n,b} \tag{19}$$

$$y_{T_{dev}}^{n,b,t} \geq T_{low}^{n,b} - T^{n,b,t} \tag{20}$$

$$y_{T_{dev}}^{n,b,t} \leq T^{n,b,t} - T_{high}^{n,b} + M_1 z_{T_{dev}}^{n,b,t} \tag{21}$$

$$y_{T_{dev}}^{n,b,t} \leq T_{low}^{n,b} - T^{n,b,t} + M_1(1 - z_{T_{dev}}^{n,b,t}) \tag{22}$$

$$T_{dev}^{n,b,t} \geq y_{T_{dev}}^{n,b,t} \tag{23}$$

$$T_{dev}^{n,b,t} \leq M_2 c_{T_{dev}}^{n,b,t} \tag{24}$$

$$T_{dev}^{n,b,t} \leq y_{T_{dev}}^{n,b,t} + M_2(1 - c_{T_{dev}}^{n,b,t}) \tag{25}$$

C. Node Constraints

Finally, the node constraints are presented below which constitute the objective function., the node power balance, and the input and output power limits. All the node constraints apply for $\forall t \in T$.

$$\begin{aligned} \min C_n = \Delta t(\sum_{t=1}^{T}(P_{im}^{n,t} C_{buy}^{t} - P_{ex}^{n,t} C_{sell}^{t})) + \sum_{j=1}^{J} E_g^{n,j} C_{ev_{pen}}^{n,j} \\ + \sum_{t=1}^{T}\sum_{b=1}^{B}(P_{pv_{dev}}^{n,b,t} C_{pv_{pen}}^{n,b}) + \sum_{t=1}^{T}\sum_{b=1}^{B}(T_{dev}^{n,b,t} C_{hp_{pen}}^{n,b} O^{t,n,b}) \end{aligned} \tag{26}$$

This work is a MILP model that has translated every objective of the EMS into a total cost to be minimized in the objective function (26). This cost comprises the minimum exchange grid power cost where P_{im}, C_{buy} the imported power and cost and P_{ex}, C_{sell} the exported power and cost, the EV unfinished charging penalty cost $C_{ev_{pen}}$, the PV curtailment penalty cost $C_{pv_{pen}}$, and finally the thermal discomfort penalty cost $C_{hp_{pen}}$.

$$\begin{aligned} P_{im}^{n,t} - P_{ex}^{n,t} = \sum_{j=1}^{J}(\frac{P_{ch}^{n,j,t}}{h_{ch}^{n,j}} - P_{v2g}^{n,j,t} h_{ch}^{n,j}) \\ + \sum_{b=1}^{B}(\frac{P_{hp}^{n,b,t}}{h_{hp}^{n,b}} + P_{l}^{n,b,t} - P_{pv}^{n,b,t}) \end{aligned} \tag{27}$$

$$\sum_{j=1}^{J}(\frac{P_{ch}^{n,j,t}}{h_{ch}^{n,j}} - P_{v2g}^{n,j,t} h_{ch}^{n,j}) + \sum_{b=1}^{B}(\frac{P_{hp}^{n,b,t}}{h_{hp}^{n,b}} + P_{l}^{n,b,t} - P_{pv}^{n,b,t}) \leq G_{in}^{n} \tag{28}$$

$$\begin{aligned} \sum_{b=1}^{B}(P_{pv}^{n,b,t} - \frac{P_{hp}^{n,b,t}}{h_{hp}^{n,b}} - P_{l}^{n,b,t}) \\ - \sum_{j=1}^{J}(\frac{P_{ch}^{n,j,t}}{h_{ch}^{n,j}} - P_{v2g}^{n,j,t} h_{ch}^{n,j}) \leq G_{out}^{n} \end{aligned} \tag{29}$$

TABLE I
PARAMETERS OF COORDINATED POWER CONTROL MODEL

Parameters	Explanation	Value
$C^{n,j}_{ev_{pen}}$	Unfinished EV Charging Penalty	10€/(1%SOC)
$C^{n,b}_{hp_{pen}}$	Thermal Discomfort Penalty	10€/(°CΔt)
$C^{n,b}_{pv_{pen}}$	PV curtailment Penalty	10€/(kW Δt)
$h^{n,j}_{ev}$	EV BMS Efficiency	case-dependent
$h^{n,j}_{ch}$	EV Charger Efficiency	case-dependent
$h^{n,b}_{hp}$	HP efficiency	0.97
$P^{n,j}_{ch_{max}}$	Charging Maximum Power	$\min(P^{n,j}_{ev_r}, P^{n,j}_{chg_r})$
$P^{n,j}_{chg_r}$	AC Charger Rated Power	22kW
$P^{n,j}_{v2g_{max}}$	V2G Maximum Power	$\min(P^{n,j}_{ev_r}, 20kW)$
$V^{n,t}$	Instantaneous Node Voltage	230V
$I^{n,j}_{ch_{max}}$	Charging Maximum Current	$\min(I^{n,j}_{ev_r}, 32\text{A})$
$I^{n,j}_{v2g_{max}}$	V2G Maximum Current	$\min(I^{n,j}_{ev_r}, 29A)$
C_b	Building Thermal Capacity	4.755 kWh/K
V_b	Building Volume	$585m^3$
C_{air}	Air Thermal Capacity	0.279 Wh/kgK
ρ_{air}	Air Density	$1.225kg/m^3$
r_b	Building Air Change Rate	$0.3h^{-1}$
$c^{n,b,t}_{p_{hp}}$	HP Coefficient of Performance	3
$T^{n,b}_{min}$	Building Minimum Temperature	17°
$T^{n,b}_{max}$	Building Maximum Temperature	27°
$T^{n,b}_{high}$	Comfort Temperature High Limit	21°
$T^{n,b}_{low}$	Comfort Temperature Low Limit	23°
$M1, M2$	Big-M Method Parameters	10
G^n_{in}	Grid Input Capacity	87kW
G^n_{out}	Grid Output Capacity	22kW

The power balance is dictated in (27) which defines that the difference between imported and exported power is total EV charging, total EV V2G power, building heating, PV rooftop generation, and base load demand ($P^{n,b,t}_l$) where $h^{n,j}_{ch}, h^{n,j}_{hp}$ the EV charger and HP efficiencies, respectively. Furthermore, (28) & (29) denote that the node composite power is always lower than the input and output node capacity limits G^n_{in} & G^n_{out}. Moreover, in that way, the node is forced to either import or export power at one time instant. Finally, for the development of the power control model without V2G capabilities, V2G variables are always zero $P^{n,j,t}_{v2g}, I^{n,j,t}_{v2g} = 0$. Finally, all parameters used for the power control are summarized in TABLE I.

IV. DATA DESCRIPTION & CASE STUDIES

In this work, the following data has been utilized by the related data sources.

1) Weather data was downloaded from Meteonorm database[1].

2)Probabilistic distributions of EV driving patterns (arrival SOC, requested energy, etc.) for Home, Semi-Public, and Public chargers were derived by the Elaad database[2] and [13]. Home chargers are typically characterized by longer parking periods and lower arrival SOCs while Semi-public and Public chargers have a higher EV arrival frequency and lower requested charging energy.

3) Load demand distribution profiles were downloaded from the mffbas database[3].

4) 3-kW rated Summer and Winter PV generation and Irradiation profiles based on [13].

5) Residential and commercial building occupancy profiles [00:00 - 08:00, 14:00- 00:00] & [09:00-21:00], respectively based on [13].

The case studies comprise three different nodes (see Table II): a Residential node with 4 home chargers and 5 residential buildings, a Commercial node with 4 semi-public/public chargers and 3 commercial buildings, and a Mixed node with 3 home chargers, 2 public chargers, 2 residential & 2 commercial buildings. Moreover, 4 cases are investigated: Cases 1 & 2 investigate the power control with and without V2G in the current scenario of 0.94 one-way charging efficiency. Cases 3 & 4 investigate the future V2G potential in actual and ideal scenarios of 0.97 & 0.99 efficiencies. It must be noted that "charging efficiency" integrates both the charger and EV battery losses ($h_{ch} * h_{ev}$). Finally, the power control was tested for the Summer and Winter seasons.

TABLE II
CASE STUDIES OF POWER CONTROL.

Nodes	Table Column Head	Seasons
Residential (Node 1)	No - Current Scenario (Case 1)	Winter
Commercial (Node 2)	Yes - Current Scenario (Case 2)	Summer
Mixed (Node 3)	Yes - Actual Future Scenario (Case 3)	
	Yes - Ideal Future Scenario (Case 4)	

V. RESULTS & DISCUSSION

In Fig. 1, the power scheduling of Node 3 is depicted for Case 1 for the Winter and Summer seasons. During Winter, most grid power is imported for EV charging and heating during the low energy prices between 19:00-05:00 and the price drop between 15:00-17:00. Additionally, PV generation is mostly exported to the grid for revenues because it coincides with the high energy price period. On the contrary, in Summer, PV generation is exported during the high energy prices between 07:00-11:00. However, the cooling of the buildings initiates earlier at noon due to the high ambient temperatures and the exploitation of the higher and more prolonged PV generation. The price drop between 14:00-17:00 is also highly taken advantage of for cooling and EV charging while the price peak at 20:00 is avoided. Hence, it can be seen that a higher percentage of PV generation is used within the node for charging and heating and the imported power is decreased.

Moreover, Fig. 2 depicts the power scheduling of Node 3 during the Winter for the V2G Cases 2 & 3. In Case 2, V2G power is rarely used due to the power losses of the 0.88 round-trip efficiency, but it can be used at low power levels for heating and EV charging at high energy prices (10:00 and 15:00). However, V2G power use is significantly

[1]https://meteonorm.com/

[2]https://platform.elaad.io/

[3]https://www.mffbas.nl/

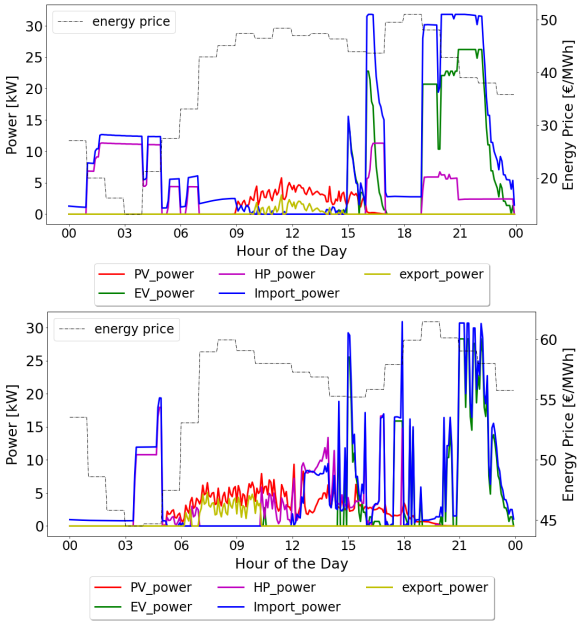

Fig. 1. Power Control at Node 3 - Case 1 - Winter (upper fig.) & Summer (lower fig.)

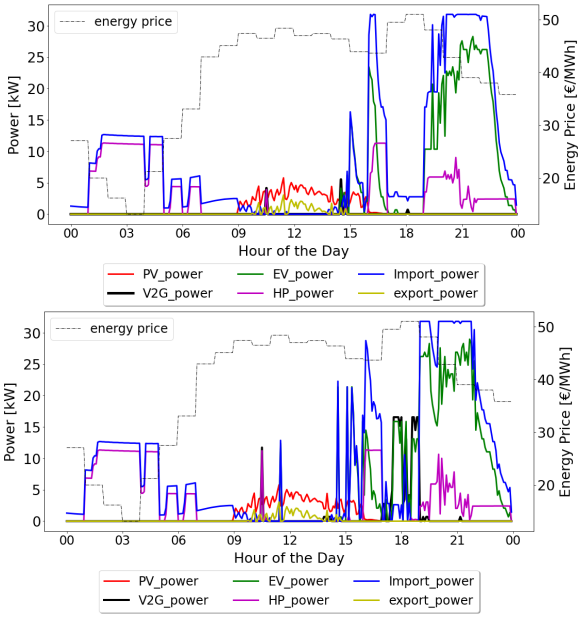

Fig. 2. Power Control at Node 3 - Winter - Case 2 (upper fig.) & Case 3 (lower fig.)

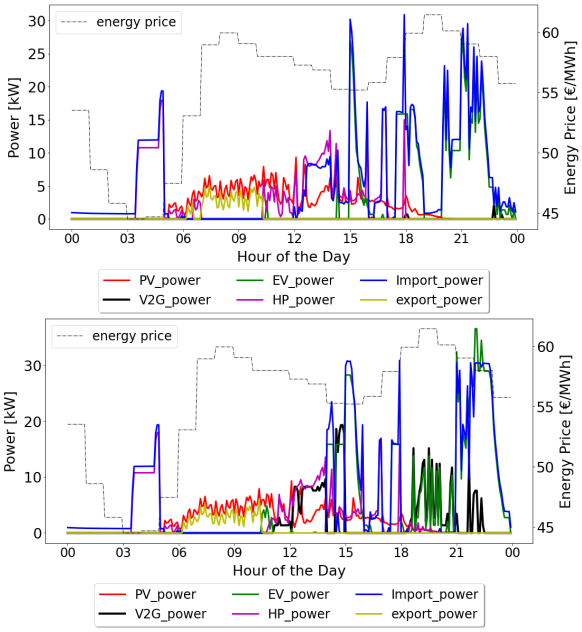

Fig. 3. Power Control at Node 3 - Summer - Case 3 (upper fig.) & Case 4 (lower fig.)

increased in Case 3 and is almost entirely responsible for other EVs charging between 17:00-19:00. Fig. 3 depicts the Summer season for Node 3 for the V2G Cases 3 & 4. During Summer, V2G is still rarely used even with the improved charger efficiency of 0.94 of Case 3. This is justified again by the higher available Summer PV generation which provides the node with higher flexibility to avoid both high energy peaks and energy losses. The use of V2G power is only increased with the ideal efficiency of 0.99 of Case 4. It is preferred against imported power between 11:00-14:00 (before the energy price drops) to cool the buildings in coordination with PV generation. Finally, it takes full responsibility for EV charging during the energy price peaks between 18:00-21:00.

Fig. 4 depicts the imported node power and V2G power use for the 4 case studies and both seasons. Residential and commercial nodes differ concerning building occupancy since residential buildings are also occupied during the night. Moreover, the charging patterns differ because EVs are usually parked in public chargers with lower parking time and higher arrival SOC than in the home chargers. Therefore, Node 2 imports significantly lower power than Node 1 due to lower requested charging energy (110kWh and 65kWh compared to 225kWh and 120kWh during Winter and Summer, respectively). Furthermore, residential buildings require more heating to respect thermal comfort, especially during the Winter nights. On the contrary, commercial buildings are mostly occupied during the day which are characterized by heating gains by solar irradiation and ambient temperature. Moreover, while imported power is slightly increased for all nodes in Case 2 due to the energy losses in the chargers by V2G use, it is notably decreased in Cases 3 & 4 due to the improved efficiencies for both seasons despite the V2G use.

Additionally, during Winter, only a minimum V2G power is used for all nodes in Case 2, which reaches up to 2kWh for a one-day simulation. However, V2G use is considerably increased with future efficiency improvements (20kWh and 28.4kWh: 19x and 27x higher for Node 3 in Cases 3 and 4, respectively). On the contrary, as in Fig. 3, the efficiency improvement of Case 3 is not enough for the utilization of V2G during Summer. Only the ideal efficiency of Case 4 could boost the V2G use, which reached up to 42kWh for Node 3. Furthermore, the low parking times of Node 2 result in the lowest V2G use ($< 0.5kWh$) due to low time flexibility.

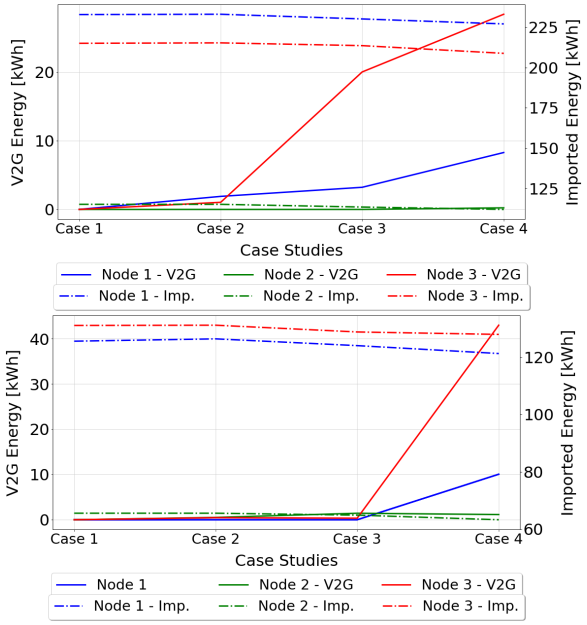

Fig. 4. Summary of Node Imported & V2G Energy during Winter (upper fig.) & Summer (lower fig.)

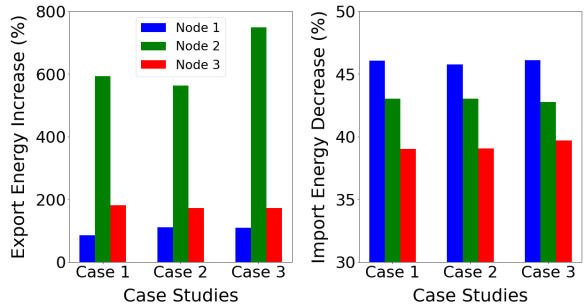

Fig. 5. Comparison of Node Import and Export Energy during Summer compared to Winter.

Finally, Figs 4 and 5 show that the imported energy amount is highly decreased during Summer due to the lower energy needed for EV charging, building cooling, and higher PV generation availability. As the right part of Fig. 5 depicts, the imported energy decreased by approximately 46%, 43%, and 39% for Nodes 1-3, respectively, and it is steady for Cases 1,2, and 3. Moreover, the higher and more prolonged PV generation has also a significant effect on the amount of exported energy which reaches up to 100%, 780%, and 190% for Nodes 1-3, respectively.

VI. Conclusions

In this work, a power control system of PV generation, electric mobility, and heating was developed and tested with and without V2G capability in different types of grids, seasons, and charger efficiencies. It was found that both chargers' efficiency and the seasonal effect have a significant impact on power scheduling, amounts of imported and exported energy, and V2G use. While with the current charger efficiencies of approximately 0.94, the V2G is rarely used for power scheduling, it can be highly increased with future improvements, especially during Winter. This is because PV generation is higher and endures significantly more during Summer providing higher flexibility in the power scheduling. Finally, it was found that the higher PV power availability and lower load consumption during Summer decreased highly the amount of imported power which reached up to 46%, An even higher effect was seen for the increase of the exported amount energy amount which reached up to 780% for the commercial grid. Moreover, the investigated grid type is important, with commercial grids importing less power and using less V2G due to lower buildings' occupancy, EVs' parking time & requested energy.

While a certain amount of uncertainty has been incorporated in the EV charging patterns, buildings' occupancy, and PV rooftop orientations, a higher level of uncertainty management with stochastic or robust optimization is recommended. Moreover, the introduction of energy storage combined with flexible loads in such power control systems can also provide valuable insights. All the above are proposed for future research.

References

[1] C. Edmunds, S. Galloway, J. Dixon, W. Bukhsh, and I. Elders, "Hosting capacity assessment of heat pumps and optimised electric vehicle charging on low voltage networks," *Applied Energy*, vol. 298, p. 117093, 09 2021.

[2] J. Gasser, H. Cai, S. Karagiannopoulos, P. Heer, and G. Hug, "Predictive energy management of residential buildings while self-reporting flexibility envelope," *Applied Energy*, vol. 288, p. 116653, 04 2021.

[3] M. Arnaudo, M. Topel, and B. Laumert, "Vehicle-to-grid for peak shaving to unlock the integration of distributed heat pumps in a swedish neighborhood," *Energies*, vol. 13, 04 2020.

[4] S. Huang and Q. Wu, "Dynamic tariff-subsidy method for pv and v2g congestion management in distribution networks," *IEEE Transactions on Smart Grid*, vol. 10, no. 5, pp. 5851–5860, 2019.

[5] F. Giordano, A. Ciocia, P. D. Leo, A. Mazza, F. Spertino, A. Tenconi, and S. Vaschetto, "Vehicle-to-home usage scenarios for self-consumption improvement of a residential prosumer with photovoltaic roof," *IEEE Transactions on Industry Applications*, vol. 56, no. 3, pp. 2945–2956, 2020.

[6] J. Hu, H. Zhou, Y. Li, P. Hou, and G. Yang, "Multi-time scale energy management strategy of aggregator characterized by photovoltaic generation and electric vehicles," *Journal of Modern Power Systems and Clean Energy*, vol. 8, no. 4, pp. 727–736, 2020.

[7] A. Mohammad, R. Zamora, and T. T. Lie, "Transactive energy management of pv-based ev integrated parking lots," *IEEE Systems Journal*, vol. 15, no. 4, pp. 5674–5682, 2021.

[8] M. Yousefi, A. Hajizadeh, M. Soltani, and B. Hredzak, "Predictive home energy management system with photovoltaic array, heat pump, and plug-in electric vehicle," *IEEE Transactions on Industrial Informatics*, vol. PP, pp. 1–1, 02 2020.

[9] W. Vermeer, G. R. Chandra Mouli, and P. Bauer, "Real-time building smart charging system based on pv forecast and li-ion battery degradation," *Energies*, vol. 13, p. 3415, 07 2020.

[10] G. R. Chandra Mouli, M. Kefayati, R. Baldick, and P. Bauer, "Integrated pv charging of ev fleet based on dynamic energy prices and offer of reserves," *IEEE Transactions on Smart Grid*, vol. PP, 05 2017.

[11] N. Damianakis, Y. Yu, G. C. R. Mouli, and P. Bauer, "Frequency regulation reserves provision in ev smart-charging," in *2023 IEEE Transportation Electrification Conference Expo (ITEC)*, 2023, pp. 1–6.

[12] N. Damianakis, G. R. Chandra Mouli, and P. Bauer, "Risk-averse estimation of electric heat pump power consumption," 06 2023, pp. 1–6.

[13] N. Damianakis, G. R. C. Mouli, P. Bauer, and Y. Yu, "Assessing the grid impact of electric vehicles, heat pumps pv generation in dutch lv distribution grids," *Applied Energy*, vol. 352, p. 121878, 2023. [Online]. Available: https://www.sciencedirect.com/science/article/pii/S0306261923012424